Ionic Liquids at air-water Interfaces

Raquel Valente (IST, SOLEIL), Eduardo J. M. Filipe (IST), Philippe Fontaine (SOLEIL)

Abstract

Ionic Liquids (ILs) are a class of new solvents considered as environmentally friendly for chemical processes. ILs consist solely of ions which asymmetric shape inhibits solidification near room temperature. In the last few years their popularity increased due to its unique properties, strongly dependent on cation and anion chosen, and therefore a large number of application have been proposed. Detailed knowledge of the ion organization at the interface of ILs can be very important and interesting to many processes.

In the present work, it is proposed to obtain a better understanding of the behaviour as well as the structure of $[C_n mim][NTf_2]$ (n=12, 14, 16, 18) ILs family at air/pure water and air/salt water interfaces through the Langmuir monolayer technique. It is presented results obtained on Langmuir monolayers of ILs by (π-A) isotherms, Brewster Angle Microscopy, Grazing Incidence X-ray Diffraction (GIXD), Total Reflection X-ray fluorescence (TXRF) and X-ray Powder Diffraction (XRD).

Key-words: Ionic Liquids, $[C_{18}mim][NTf_2]$, Langmuir Monolayer, X-ray, interfaces.

I. Introduction

Ionic liquids (ILs) are salts with melting point much lower than usual salts, $T_m \leq 100^{\circ}C$, i.e., below the boiling point of water; some of them even melt below 0˚C. Some authors also differentiate ILs from Room-Temperature Ionic Liquids (RTILs), which melt at temperatures below 25 ˚C. These ILs, in contrast with salt solution, consist entirely of cations and anions, without a presence of any solvent. Until one hundred years ago, it was never imagined that, at room temperature, ions could form a liquid unless diluted in a solvent. [1], [2] When comparing a typical IL with a typical inorganic salt, with single or few atom cations and anions, the clear difference between both is their chemical structure. ILs show an asymmetric shape, which results in a destabilization of the crystalline lattice, reducing the melting point and increasing the liquidus range of the IL. [3]

The popularity of ILs increased in last years, mainly because of two advantages over traditional solvents:

- They are considered as an environmental friendly alternative to the volatile organic compounds (VOCs) used as a solvent in industry. When compared to VOCs, ILs typically have very low volatility, due to their strong ionic (coulomb) interaction: their vapor pressures are extremely low and have to be obtained at very high temperatures, therefore information about their vapor pressures are scarce in the literature. [4] ILs have other advantageous properties, such as, nonflammable, high viscosity, thermal stability, ability to dissolve a wide range of compounds, controlled miscibility with organic solvents and a wide electrochemical window. Beyond that they can be frequently recycled [4], [5];
- The properties of ILs strongly depend on the cation and anion chosen. There are around one million possible combinations that can be made to obtain the desirable properties.

Indeed, all these unique properties are the reason of the increase of the number of publications concerning ILs in the last years and therefore of the number of applications of ILs. ILs have been studied for different applications such as in medicine [6]; as a solvent in industry, both in chemical and enzymatic biocatalysis [4], [7], [8]; as an electrolyte [9]–[12], among other applications.

For a potential application of processes at interfaces, ILs are often involved but poorly investigated from a fundamental point of view. The knowledge of the ion organization at interfaces and its interfacial properties can be very important. ILs with long alkyl chain are amphiphilic molecules, with a hydrophobic and a hydrophilic part, thereby it should be notice that they can show a similar behaviour to those shown by ionic surfactants forming structures as micelles. Thus, this type of ILs could also form Langmuir monolayers, a molecular thick layer of amphiphilic molecules, with the hydrophilic head groups down and the hydrophobic tail groups up, that can be studied through Langmuir techniques. Despite their great potential, this area is a largely unexplored field:

- Bai *et al.* [13] reported synthesis of a gold nanoparticles in a two-phase liquid/ liquid system, using S-3-hexadecyl-1-(2- hydroxy-1-methylethyl) imidazolium bromide ($[C_{16}hmim]Br$) as a monolayer-stabilizer;
- Later, Jia *et al.* [14] prepared Gold nanochains at the air/ water interface, using 1-hexadecyl-3-methylimidazolium bromide ($C_{16}mimBr$) as a monolayer-stabilizer.
- Mukherjee *et al.* [15] reported the study of solution and surface chemical behaviour of triisobutyl(methyl)phosphonium tosylate ($[P_{1,4,4,4}][tos]$) and trihexyl(tetradecyl)phosphonium bis 2,4,4-(trimethylpentyl)phosphinate ($[P_{66614}][(iC_8)_2PO_2]$). Langmuir Monolayer formation is addressed;
- Tamam *et al.* [5] reported the study of a Langmuir film of 1-butyl- 1-methyl pyrrolidinium tris(pentafluoroethyl) trifluorophos phate ([BMPL][FAP]) on mercury;
- Recently, Filipe *et al.* [16] reported the formation of Langmuir films of $[C_{18}mim][NTf_2]$ at air/ water

interface. Molecular dynamics simulation supported experimental results.

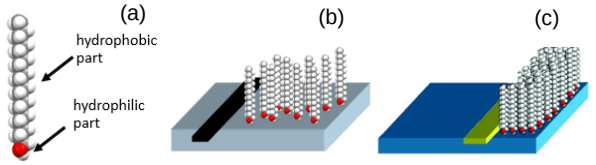

Figure 1 – Amphiphilic molecule (a) and Langmuir Monolayer at large areas (b) and at small areas (c).

In the present project, it is proposed to study the behavior of six different ionic liquids with one long chains and its structure at the air/pure (A/PW) and air/salt water (A/SW) interfaces. The cations that were chosen are imidazolium based ($[C_nmim]^+$, n=12, 14, 16 and 18). It was chosen a family of ionic liquids with a long chain that showed to give the insoluble character mandatory for an amphiphilic molecule. Moreover, the studies about its Langmuir monolayer are scarce even though imidazolium IL are one of the most considered IL for applications. It was chosen three different anions: a smaller one (Cl^-), another small but bigger than Cl^- (PF_6) and finally a non-sperical one with internal mobility ($(CF_3SO_2)_2N=NTf_2$). Those were chosen to study different types of combinations.

In Table 1 are listed the film-forming substances used in this work, their origin, reported purity and the concentration used in spreading solution and the spreading solvent (chloroform) used in the solutions, its origin and reported purity. The through used has a compression ratio, i.e. ration between the maximum and minimum area, of 3.

The behaviour of those six ionic liquids and their structure at the A/PW and A/SW interfaces were studied at different length scales: macroscopic, by surface tension measurements; microscopic, by images obtained by Brewster Angle Microscopy (BAM); and nanometric and molecular, by x-ray scattering, Grazing Incidence X-ray Diffraction (GIXD), Total Reflection X-ray fluorescence (TXRF) and X-ray Powder Diffraction (XRD). All the experiments in the present project were carried out at SIRIUS beamline (Soft Interfaces and Resonant Investigation on Undolator Source) in Synchrotron facility (SOLEIL) in Orsay, France.

II. Results and Discussion

II.1. Langmuir Isotherms

First, it was studied the stability of different substances at two different interfaces: A/PW and A/SW. For the SW subphase, it was used 0.02 M of NaCl. All experiments were performed at 20°C; the ILs solution volume used was 75 µL; three different relaxation times were used (10 minutes, one night and one weekend) as well as three different compression rates (20, 36 and 69 cm^2min^{-1}; respectively 0.0002, 0.0004 and 0.0008 nm^2sec^{-1} $molecule^{-1}$). It is considered that the surface pressure does not change, when it varies less than 1.5 mNm^{-1}. During the experiments, it was calculated the difference of areas between each compression, shown by the shift of the isotherm to smaller areas per molecule, called loss in area.

1. $[C_{18}mim][NTf_2]$

Pure Water (PW): First, the (π-A) isotherm of $[C_{18}mim][NTf_2]$ was studied for 3 different relaxation times and three different compression rates.

10 minutes. After deposition of the monolayer and 10 minutes for solvent evaporation, the compression was performed at a compression rate of 20 cm^2min^{-1} (ISOT1860). The isotherm that represents the compression/ decompression cycles made is shown on Figure 2. For the first compression, the isotherm shows a first increase of surface pressure over a large range of area per molecule, followed by an appearance of a plateau-like region at 24.0 mNm^{-1}. It is possible to consider that this monolayer is considerably compressed, due to the gradual increase in surface pressure up to 0.27 $nm^2molecule^{-1}$. The plateau region, a highly compressible region, appears at small molecular areas (0.27-0.17 $nm^2molecule^{-1}$). On first expansion, it is possible to see that the isotherm shifted to smaller surface pressures/ molecular areas and a plateau also exists but it appears at 14.5 mNm^{-1} and different molecular areas from the compression (0.22-0.35 $nm^2molecule^{-1}$).

Several compression/ decompression cycles were made to study the reproducibility of the (π-A) isotherm after more than one cycle. In the second and third compression, it is observed a decrease of the plateau size (0.22-0.17 and 0.18-0.17 $nm^2molecule^{-1}$, respectively), that is inexistent at fourth; the highest pressure is reached in the third compression (24.3 mN m^{-1}). From the fourth to seventh compression, the maximum surface pressure reached decreases at each compression made. Although, starting at the same surface pressure and molecular area as the first expansion, on the next expansions, it is observed a decrease on the plateau size (ΔA_{exp2}=0.06 nm^2 $molecule^{-1}$; $\Delta A_{exp\ 3}$=0.03 $nm^2molecule^{-1}$) appearing only until third expansion, alike in compressions.

To study the effect of compression rate on the isotherm, two isotherms were made with compression rates of 36(ISOT18120) and 69cm^2min^{-1} (ISOT18240). Comparing to ISOT1860, all the compressions of ISOT18120 also present a gradual increase of surface pressure, followed by the appearance of a plateau. The maximum surface pressure is reached on seventh compression and it is higher (26.5 mNm^{-1}). Although there is a decrease of plateau size as in ISOT1860, in ISOT18120 it is bigger and appear until seventh compression, at least. On every expansion is seen a plateau at 15.0mNm^{-1}, beginning at 0.2$nm^2molecule^{-1}$, approximately. The plateau size of each expansion is bigger than the correspondent plateau size of each expansion of ISOT1860 and appears at bigger molecular areas.

Table 1 – Film-forming substances and spreading solvent used in this work, their origin, purity and concentration.

Name	Formula	Origin	Purity	Concentration	
				mmol/L	mg/mL
1-dodecyl-3-methylimidazolium bis(trifluoromethylsulfonyl)amide	$C_{18}H_{31}F_6N_3O_4S_2$	Iolitec	>98%	2.5	1.33
1-tetradecyl-3-methylimidazolium bis(trifluoromethylsulfonyl)amide	$C_{20}H_{35}F_6N_3O_4S_2$	Iolitec	>98%		1.40
1-hexadecyl-3-methylimidazolium bis(trifluoromethylsulfonyl)amide	$C_{22}H_{39}F_6N_3O_4S_2$	Iolitec	>98%		1.45
1-octadecyl-3-methylimidazolium bis(trifluoromethylsulfonyl)amide	$C_{24}H_{43}F_6N_3O_4S_2$	Iolitec	>98%		1.54
1-octadecyl-3-methylimidazolium chlorine	$C_{22}H_{43}ClN_2$	Iolitec	>98%		0.93
1-octadecyl-3-methylimidazolium hexafluorophosphate	$C_{22}H_{43}F_6N_2P$	Iolitec	>98%		1.20
Chloroform	$CHCl_3$	VWR Chemicals	G.C.	-	

Regarding ISOT18240, its isotherms shifts to higher molecular areas and surface pressures, comparing to ISOT18120; all compression plateaus have bigger size than both ISOT1860 and ISOT18120, but the maximum surface pressure, reached on the first compression, is lower than ISOT18120 (26.0 mNm^{-1}). ISOT18240 presents a major difference, relatively to the other two: two plateaus on first and second expansion. The first one appears on the beginning of the expansions (24.7 mN m^{-1},0.17 $nm^2molecule^{-1}$; ΔA_{exp1}=0.06nm^2 $molecule^{-1}$; ΔA_{exp2}=0.01 $nm^2molecule^{-1}$); the second appears at 14.5 mNm^{-1} and on the first compression at bigger areas than the second (0.43-0.31 $nm^2molecule^{-1}$ and 0.38-0.25 $nm^2molecule^{-1}$, respectively). All the next expansions present a single plateau starting at 0.22 $nm^2molecule^{-1}$ and at 14.5 mNm^{-1}.

The shift of the isotherms and the decrease of the plateau size and of the maximum surface pressure reached indicate a loss in area at each compression. In Table 2 are listed the loss in area at each compression for [C_{18}mim][NTf_2].

Night. The first compression was made after waiting one night (≈15 hours) at a compression rate of 20 cm^2min^{-1} (ISOT18N). Comparing with ISOT1860, the first compression reaches a higher value of maximum surface pressure (23.8 mNm^{-1}) and all the isotherm shifts to smaller surface pressures/ molecular areas and the plateau disappears, even in the first compression. In the following compressions, the isotherm does not show an increase of surface pressure until molecular area of 0.4 $nm^2molecule^{-1}$ approximately is reached. Afterward it is observed a gradual increase of surface pressure over molecular area until it is reached its maximum value. Moreover, the isotherm dislocates to smaller values of surface pressure/molecular areas with the compression, suggesting loss in area as in the isotherm after 10 minutes of solvent evaporation (Table 2). At the expansions, the isotherm shifts to smaller surface pressures/ molecular areas, not showing any plateau.

Weekend (WE). For this molecule, the last Langmuir experiment was made after waiting a WE (≈65hours) at a compression rate of 20 cm^2 min^{-1} (ISOT18WE). This isotherm shifts to even smaller surface pressures/ molecular areas than ISOT18N; and the maximum surface pressure reached is the smallest for this compression rate, 13.0 mNm^{-1}. As with ISOT18N, the gradual increase of surface pressure is only observed when it is reached approximately 0.35 $nm^2molecule^{-1}$ in all the compressions. Both compression and expansion do not present plateau. Loss in area is shown in Table 2.

SW: [C_{18}mim][NTf_2] was also study at A/SW interface. As in PW, the molecule on NaCl subphase was studied for three different relaxation times and three different compression rates. Table 2 shows the loss in area of each isotherm for this subphase.

10 minutes. After a wait of 10 minutes for solvent evaporation, compressions were performed at three compression rates: 20 (ISOTS1860; Figure 3), 36 (ISOTS18120) and 69 cm^2min^{-1} (ISOTS18240). All of them show a similar behavior, comparable to the ones performed at A/PW interface, a gradual increase of surface pressure in the beginning of the compression, followed by an appearance of plateau at larger surface pressure comparing to the corresponding ones at PW subphase. Although when compression rate is increased the isotherm shifts to lower area per molecule, it is also visible that at each compression the isotherms shifts to lower areas per molecule. A plateau is visible at the beginning of each expansion (only 1st compression of ISOT1860), followed by a gradual decreasing of surface pressure.

Night. After wait one night for solvent evaporation, compression was performed at 20 cm^2min^{-1} (ISOTS18N). Although ISOTS18N shifts to smaller surface pressure/ molecular areas, its behavior is similar to the isotherms performed after a wait of 10 minutes (gradual increase of surface pressure followed by a plateau) and it is reached a higher maximum surface pressure. Until the fourth compression/ decompression cycle, a plateau is observed; the one present in the expansions begins at the same surface pressure and molecular area.

WE. The last experiment was performed at 20 cm^2 min^{-1} after wait one WE (ISOTS18WE). Although this isotherm reaches similar maximum surface pressures comparing to others at the same interface, the value is the smallest. As in the PW, ISOTS18WE shifts to smaller surface pressures/ molecular areas than ISOTS18N and both compression and decompression do not present plateau.

When comparing loss in area at A/PW and A/SW interfaces (Table 2), it is shown bigger losses at the A/PW interface, corroborating the fact that the addition of salt stabilizes the monolayer formed. Moreover, the maximum surface pressure reached is higher.

2. [C_{16}mim][NTf_2]

PW: The experiments were performed for 2 solvent evaporation times and 3 compression rates.

10 minutes. Starting with experiments after a wait 10 minutes for solvent evaporation at three different compression rates: 20, 36 and 69 cm^2min^{-1} (ISOT1660, ISOT16120 and ISOT16240). As [C_{18}mim][NTf_2], at each compression there is a shift of the isotherm to smaller surface pressure/ molecular areas, but contrary to [C_{18}mim][NTf_2], [C_{16}mim][NTf_2] does not form plateaus when compressed, not even at the first compression, showing just a gradual increase of surface pressure, observed at lower molecular areas. The highest maximum surface pressure is reached on ISOT16240 (21.8 mNm^{-1}), lower than the maximum surface pressure of ISOT1860. The loss in area can be compared on Table 2, confirming that [C_{18}mim][NTf_2] form more stable monolayers at this interface than [C_{16}mim][NTf_2].

Night. Then it was performed experiments after a wait of one night. Knowing that at each compression made, after a wait of 10 minutes, there is a big shift of the isotherm to smaller surface pressures/molecular areas, it was decided to test ISOT16N at three different compression rates (ISOT16N60: 20, ISOT16N120: 36 and ISOT16N240: 69 cm^2min^{-1}). It was concluded that [C_{16}mim][NTf_2] is not stable after waiting one night for solvent evaporation since no surface pressure increase is observed during compression, regardless of the compression rate used. From this results obtained, it was decided not to do the experiment after waiting a WE.

SW: As said before at A/SW interface all the experiments done with [C_{18}mim][NTf_2] were also performed with [C_{16}mim][NTf_2].

10 minutes. The experiments performed after a wait of 10 minutes for solvent evaporation at A/SW interface (ISOTS1660: 20, ISOTS16120: 36 and ISOTS16240: 69 cm^2min^{-1}). All present a similar behavior comparing to ISOT1660, ISOT16120 and ISOT16240: increase of surface pressure during all the compression; shift of the isotherm to smaller surface pressure/ molecular areas and no plateau formation during compressions; and the highest maximum surface pressure is reached on ISOTS16240 (31.8 mNm^{-1}). As the isotherms performed in the A/PW interface the surface pressure increase occurs at lower molecular areas at each compression made.

Night. The experiment after a wait of one night (ISOTS16N) was performed at 20 cm^2min^{-1}. Despite the similar behavior comparing this isotherm to the one performed after 10 minutes of wait, the increase of surface pressure occurs when it is reached 0.40 nm^2 $molecule^{-1}$ for the first and 0.3 $nm^2molecule^{-1}$ for the following compressions and the maximum pressure of 13.4 mNm^{-1} is reached.

WE. The isotherm performed after one WE (ISOTS16WE) at 20 cm^2min^{-1} has a similar behavior to the ones performed at the same interface, however at the first compression the increase of surface pressure occurs at 0.32 $nm^2molecule^{-1}$ and on the following ones at 0.30 $nm^2molecule^{-1}$ and the maximum pressure reached is 8.9 mNm^{-1}.

From the results it can be concluded that [C_{16}mim][NTf_2] are less stable than [C_{18}mim][NTf_2] on both subphases. It can be corroborated from the Table 2 where it is shown that for [C_{16}mim][NTf_2], the loss in area is bigger when compressed (when the same conditions are used). Thus, it is demonstrated that with the decrease of the hydrophobic tail, the stability of the film decreases. The existence of the shift of the isotherm to smaller areas per molecule, i.e. loss in area, could suggest that the molecules are disappearing from the surface by dissolution in water

3. [C_{14}mim][NTf_2] and [C_{12}mim][NTf_2]

Regarding A/PW interface, experiments were performed after 10 minutes: at three compression rates for [C_{14}mim][NTf_2] (ISOT1460; ISOT14120; and ISOT14240); and [C_{12}mim][NTf_2] at 36 (ISOT12120) and 69 cm^2min^{-1} (ISOT12240). At A/SW, ISOTS1460, ISOTS14120 and ISOTS14240 were performed.

PW: [C_{14}mim][NTf_2]**.** At 20 cm^2min^{-1}, the compression of the film does not induce an increase of surface pressure; as opposed to others rates used, which shows an increase of surface pressure that begins at 0.25 $nm^2molecule^{-1}$ approximately. The highest surface pressure (2.4 mNm^{-1}) is reached when the fastest compression rate is used (69 cm^2min^{-1}), despite the values obtained for both compression rates (36 and 69 cm^2min^{-1}) are not very different (1.6 and 2.4 mNm^{-1}, respectively). Both isotherms present a maximum surface pressure smaller than the value of surface pressure measured after spreading.

[C_{12}mim][NTf_2]. At this interface, only ISOT12120 and ISOT12240 were performed, since ISOT1460 didn't show any variation when compressed. By the previous results, it was concluded that the molecule became less stable with the decrease of the hydrophobic tail, so no change will be expected during compression of this molecule. Oppositely to [C_{14}mim][NTf_2] when [C_{12}mim][NTf_2] is compressed, no increase of surface pressure is observed, regardless of the compression rate used.

SW: [C_{14}mim][NTf_2]. ISOTS1460 was the first isotherm performed at this interface. At 20 cm^2 min^{-1}, this molecule shows a small increase of surface pressure when compressed for the first time and in the following compressions no increase is observed. Though it is observed an increase of surface pressure, the maximum surface pressure reached (3.5 mNm^{-1}) is smaller than the value measured right after deposition of the film (6.1 mNm^{-1}).

At 36 cm^2min^{-1}, it is observed an increase of surface pressure at the first (8.9 mNm^{-1}) and a smaller increase at second compression (3.7 mNm^{-1}), smaller than the value measured after film deposition (7.3 mNm^{-1}). At 69 cm^2min^{-1}, it is observed an increase at the three first compressions. The pressure reached in the first compression (10.4 mNm^{-1}) is the highest value reached with this molecule; at the second and third compression, the values reached are smaller (5.3 and

3.5 mNm^{-1}, respectively) than the value measured after spreading (6.4 mNm^{-1}).

By the results, it can be concluded that [C_{14}mim][NTf_2] and [C_{12}mim][NTf_2] are not stable at A/PW interface. Although there is an increase of [C_{14}mim][NTf_2] stability at A/SW interface, this molecule is less stable than [C_{18}mim][NTf_2] and [C_{16}mim][NTf_2].

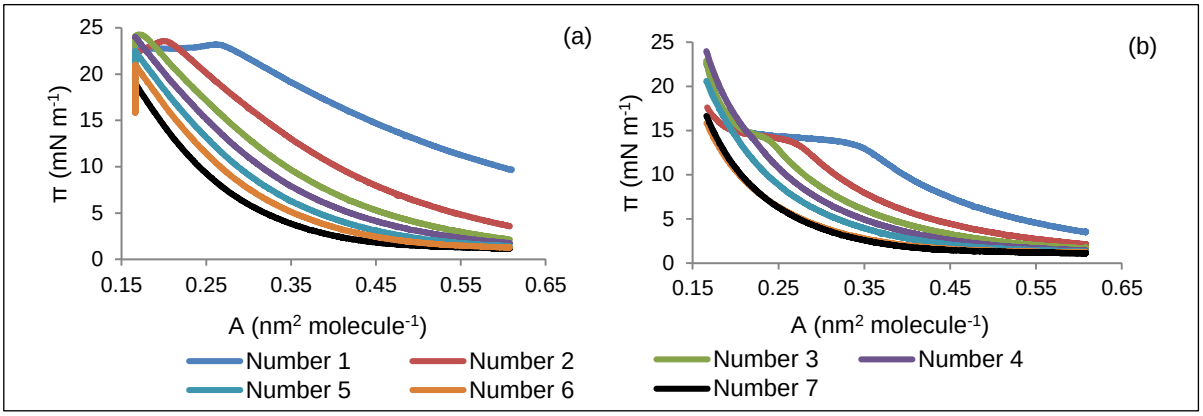

Figure 2 – ISOT1860 – Seven compression/decompression cycles : (a) Compressions ; (b) Decompressions. Isotherm performed at A/PW interface, after 10 minutes of solvent evaporation at a compression rate of 20 cm^2 min^{-1}.

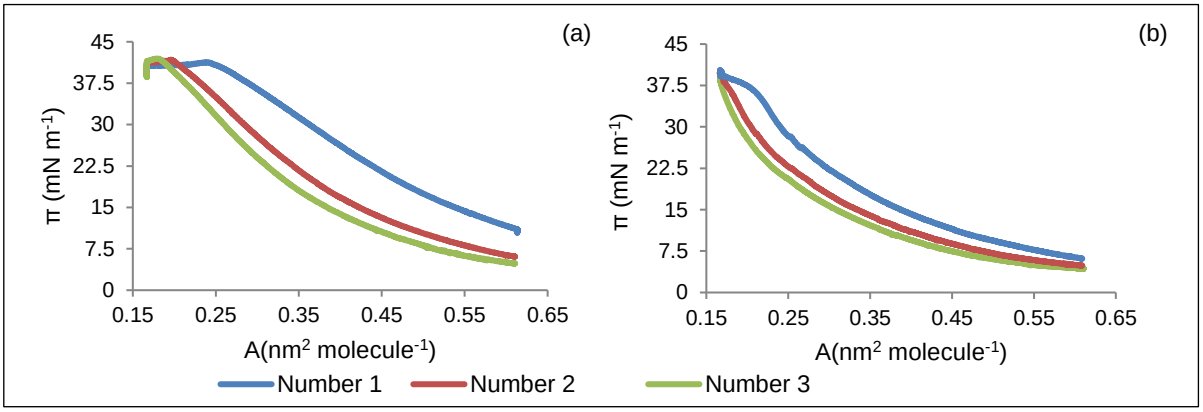

Figure 3 – ISOTS1860 – Three compression/decompression cycles : (a) Compressions ; (b) Decompressions. Isotherm performed at A/SW interface, after 10 minutes of solvent evaporation at a compression rate of 20 cm^2 min^{-1}.

Table 2 – Losses in area at each compression for the different isotherms.

Isotherm	P	Compression						
		2	3	4	5	6	7	8
ISOT1860	15	28%	38%	43%	48%	51%	56%	-
ISOTS1860	15	21%	29%	-	-	-	-	-
ISOT18120	15	21%	30%	35%	40%	43%	46%	48%
ISOTS18120	15	18%	26%	18%	19%	36%	38%	39%
ISOT18240	15	16%	23%	28%	32%	35%	38%	40%
ISOTS18240	15	18%	24%	28%	-	-	-	-
ISOT18N	10	10%	17%	22%	26%	-	-	-
ISOTS18N	10	13%	19%	-	-	-	-	-
ISOT18WE	8	4%	6%	12%	13%	15%	-	-
ISOTS18WE	8	11%	15%	23%	-	-	-	-
ISOT1660	6	41%	52%	-	-	-	-	-
ISOTS1660	6	33%	42%	50%	-	-	-	-
ISOT16120	1	-	29%	40%	46%	53%	58%	-
	3	43%	60%	65%	-	-	-	-
ISOTS16120	6	24%	32%	37%	41%	-	-	-
ISOT16240	3	31%	43%	52%	58%	63%	67%	69%
ISOTS16240	6	22%	28%	33%	36%	39%	41%	42%
ISOTS16N	6	11%	14%	18%	23%	-	-	-
ISOTS16WE	6	5%	7%	9%	12%	-	-	-

4. [C_{18}mim][Cl] and [C_{18}mim][PF_6]

The isotherms of [C_{18}mim][Cl] and [C_{18}mim][PF_6] were performed after 10 minutes at A/PW interface and at a compression rate of 20 cm^2min^{-1}. Two compression/ decompression cycles were made for each molecule, during which both show a variation of surface pressure of 0.3 mNm^{-1} approximately, allowing to consider no variation during the process. Therefore, it can be concluded that both molecules do not form stable monolayers at this interface.

5. Equilibrium Spreading Pressure Measures

As said above, the Equilibrium Spreading pressure, ESP, is defined as the equilibrium pressure between the film and its bulk phase. The bulk phase was placed on the subphase in study (PW or SW) and π was monitored with time until it reached the saturation, the ESP value. The ESP was measured at a constant area and all substances studied are solids, except [C_{12}mim][NTf_2] which is a liquid at working temperature. In Table 3, it is shown the ESP values for each substance and subphase studied.

Table 3 – ESP value for the different molecules.

Molecule	ESP (mNm^{-1})	
	PW	SW
[C_{18}mim][NTf_2]	13.8	23.3
[C_{16}mim][NTf_2]	16.7	36.2
[C_{14}mim][NTf_2]	29.7	39.4
[C_{12}mim][NTf_2][1]	26.3	28.9

There is a correlation in both subphases (Table 3) between the value of ESP measured and the increase of the hydrophobic tail of the molecules (with the $[NTf_2]^-$ anion): increasing the hydrophobic tail, the ESP value diminishes. The increase of the tail increases the hydrophobicity of the molecules leading the film-forming to spread fewer molecules into the surface affecting less the surface tension of the subphase, resulting in a lower ESP value. As such [C_{18}mim][NTf_2] has the lesser value of ESP.

Since [C_{12}mim][NTf_2] has a smaller hydrophobic tail and the same anion, it would be expected to have a smaller value for ESP, when compared to the value of [C_{14}mim][NTf_2]. However, that doesn't happen since the molecule is a liquid and it can't be compared with the value measured for solid molecules so it does not fit the correlation. Moreover, since this molecule has a smaller chain, dissolution can not be excluded.

6. Equilibrium Isotherm

All the (π-A) isotherms show a shift of the curves to smaller areas per molecule which can be attributed to the disappearing of the molecules by dissolution or even irreversible crystal formation. However, it is not possible to confirm that this disappearance is complete. To confirm such hypothesis, for a fixed surface pressure, it was taken the measured values of area per molecule of each compression and then plotted along time. The experimental curve is then fitted with the function $A = A_0 + constant \times e^{\frac{constant}{t}}$. Since the constant A_0 is different from zero, it can be concluded that, if an infinite number of cycles were made, the isotherm would reach an "equilibrium isotherm" made of the (A_0, π) points.

7. Conclusions of macroscopic measurements

- The addition of salt to the water stabilizes the monolayer, increasing the surface pressure comparing to experiments at PW subphase. At A/SW, the maximum pressure reached is higher, it is more likely to find plateaus and the loss in area per compression is lesser (Table 2);
- [C_{18}mim][Cl] and [C_{18}mim][PF_6] are not stable at A/PW interface;
- The stability of [$C_n$mim][NTf_2] follows the same behavior as fatty acids (higher n=greater stability):
- On PW, [C_{14}mim][NTf_2] and [C_{12}mim][NTf_2] proved to form instable monolayers. On SW, [C_{14}mim][NTf_2] showed a small enhance of stability;
- Although [C_{18}mim][NTf_2] is the molecule that forms more stable monolayers, [C_{16}mim][NTf_2] forming-films are also stable on both subphases;
- [C_{18}mim][NTf_2] is the molecule with the lesser ESP;
- The loss in area attributed to a loss of molecules by dissolution seems to be more complex, as proven by the existence of an equilibrium isotherm.

The next experiments were done just for [C_{18}mim][NTf_2] since it proved to form more stable monolayers.

II.2. Brewster Angle Microscopy (BAM)

BAM technique was used to complement the results/ interpretations obtained with Langmuir Isotherms at a smaller length scale. BAM images were obtained at PW and SW interface along cycles. The BAM images was recorded for 2 different relaxation times at low surface density (10 minutes and 1 night); though, experiments for 1 night did not show any formation of structures or domains. Next, only results for 10 minutes are present.

PW: Figure 4 shows BAM images recorded. At large areas on the first compression, it was expected to find circular domains [16]; however, no domains were detected (Figure 4 (a)). This can be due to a camera contrast problem that persisted during all the experiments (with SW subphase included) causing poor contrast and, consequently, difficulty to observe existent domains.

On compression, it is observed that the brightness of the image increases uniformly. As the plateau is reached brighter spots are observed (Figure 4 (b)). Those spots are associated to crystalline-like or at least 3D (not monolayer) structures and indicates a thicker film. The structures observed are growing until the end of the plateau and expansion is initiate (Figure 4 (c)). Those structures can be attached to the formation of multilayers, as suggested before. [12]

During all the expansions, the structures seem to vanish until no domain are visible. Those structures seem to be big structures vanishing, before the plateau is reached (Figure 4 (d)); then, it is possible to detect some fractured on the plateau, just until its end (0.36 $nm^2molecule^{-1}$; Figure 4 (e)), when they totally fracture and only small circular domains are found on the surface (Figure 4 (f)). Then, these small domains gradually disappear from the BAM image.

[1] Molecule Liquid.

A second compression was made to study the film when compressed again. In the beginning of compression, no domains are observed, but when it is reached an area of approximately 0.35 nm^2 $molecule^{-1}$, small circular domains are found (Figure 4 (g)). When the plateau is reached, bigger domains are observed, smaller than the ones found on the first compression (Figure 4 (h)). Although these domains were found, it is not possible to see them on the BAM images. This can be due again to the poor camera contrast. Alternatively, it may be because these are less thick and dense than those found before, which can cause less reflectivity of the light, resulting in poor contrast. During expansion, as on first compression, the domains get smaller and disappear.

The last compression just show small domain (smaller than the ones on the second) (Figure 4 (i)). Those domains could be considered as some residual domains that did not disappeared before.

The existence of bright spots and thicker film suggests the existence of a monolayer in coexistence with multi-layered structures, on the first two compression/ decompression cycles. As said before, the alkyl side chains (hydrophobic tail groups) are oriented towards air, so it is preferable the formation of monolayers or trilayers comparing to the formation of bilayers or tetralayers. [16] On all the compressions, the appearance of the domains only happened above the plateau present on the expansions.

In addition of the problem with camera contrast, the difficulty in obtaining images can be due the fact that the area recorded (500 µm x 700 µm) by the camera is small relatively to the area of the Langmuir trough used, resulting in an area not recorded. Since this area not registered were bigger, some existing domains could not appear on the recorded area.

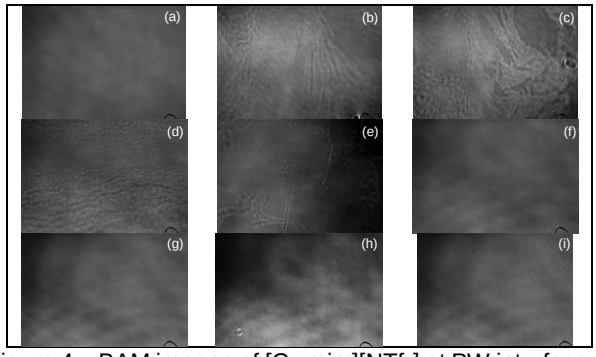

Figure 4 – BAM images of [C_{18}mim][NTf_2] at PW interface at various stages of the compression/decompression cycles.

SW: BAM images recorded for SW subphase are present on Figure 5.

At the beginning of the first compression, no domains were observed (Figure 5 (a)). This can be due to the camera poor contrast or absence of domains. However, by the results of Filipe, E. et al [16] on PW and since the addition of salt to the subphase stabilizes the monolayer, it was expected to observe some domains. Though, since no literature exists for [C_{18}mim][NTf_2] on this specific subphase, it is not possible to confirm that domains are supposed to be found. As in PW, the image gets brighter, along the compression. Due to the poor camera contrast causing an unclear image, it was not possible to identify when domains start to appear. However, when the plateau was reached, small circular domains were observed (Figure 5 (b)). These were in larger number but smaller in size than the ones on the second compression on PW. Since the spreading of a monolayer onto SW can result in a monolayer where crystalline areas and dense agglomerates coexist [17], it can be supposed that the crystalline areas could have less density than the small agglomerates. Despite the appearance, it was not observed the vanishing of these domains, during the expansion; although, on 0.36 $nm^2molecule^{-1}$ and 21 mNm^{-1} approximately (near ESP value), it was possible to see some structures (Figure 5 (c)), but the image was not very clear. From this point of expansion, no domains or structures were captured (Figure 5 (d)).

At second and third compression, no domains were seen (Figure 5 (e)); however, domains that may exist on the second compression could be very small and difficult to observe due to camera resolution.

As on PW, it is suggested the existence of a multi-layer structured on SW by the results. The difficulty to observe the domains/ structures in any of the compressions may be due to a combination of several reasons: (i) poor camera contrast and low camera resolution; (ii) very small domains; and (iii) small area recorded compared to the Langmuir trough area.

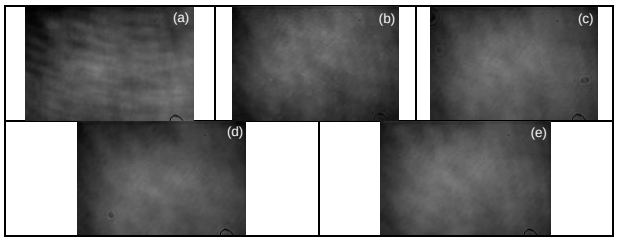

Figure 5 – BAM images of [C_{18}mim][NTf_2] at SW interface at various stages of the compression/decompression cycles.

II.3. X-ray Experiments

1. Grazing Incidence X-ray Diffraction and Powder Diffraction

[C_{18}mim][NTf_2] Langmuir monolayer was also studied at molecular level by GIXD. Due to the non-stability of the films at high surface pressures, the films were continuously compressed during each scan. The GIXD diffraction peaks for the molecule were fitted with Lorentzian line shape. This experiment was used to study the monolayer on PW, for 1 and for 3 compression/ decompression and on SW along an isotherm.

First, it was studied on PW during the first compression. Since it was not known where were expected to find peaks, the GIXD scans were taken on different intervals: experiment 1 in the interval between Q_{xy}=13.0 nm^{-1} and 18 nm^{-1}; the 2nd and 3rd between Q_{xy}=13.0 nm^{-1} and 16.5 nm^{-1}; and the 4th in Q_{xy}= 7 - 8.2 nm^{-1}. It was performed 4 experiments at different volumes, compression rates and relaxation times. From those experiments, it was possible to conclude that there are at least 4 peaks in the powder patterns for each value of inverse surface density,

Q_{xy}=7.6 nm^{-1}, Q_{xy}=14.9 nm^{-1}, Q_{xy}=15.1 nm^{-1} and Q_{xy}=15.3 nm^{-1}.

Then, the monolayer was studied for the next compressions/ decompressions cycles. The intervals for the next experiments were chosen considering the value of the peaks obtained before: 5th and 7th experiments were taken between Q_{xy}=11.0 nm^{-1} and 17nm^{-1}; and 6th in the interval of Q_{xy}= 11 – 14.5nm^{-1}. The peak Q_{xy}=15.3 nm^{-1} was only found on 2nd and 3rd compression, though this has been the only one that was also found on these experiments. On the first compression/ decompression (5th and 6th experiment) as well as on the other compressions, other peaks were found, Q_{xy}=11.9nm^{-1}, Q_{xy}=12.2nm^{-1}, Q_{xy}=12.7 nm^{-1} and Q_{xy}=12.9 nm^{-1}. The striking point of these data is that all the peaks found were obtained above the ESP value (13.8 mN m^{-1}) and no peaks were found below this value.

From GIXD, besides the parameters obtained above, it is obtained a Q_z - Q_{xy} map of the diffraction data (Figure 6 (b)). This map shows that the diffraction along Q_z, i.e. vertically, do not looks like 2D diffraction but to powder or multilayer diffraction. Indeed, some peaks looks like part of diffraction rings (3D powder) and some other are narrow in Q_z (multilayers). In addition to GIXD, it was also performed Powder diffraction of [C_{18}mim][NTf_2] on bulk form, using an wavelength of 1.18 Å. From the results of the experiments it can be concluded that some peaks obtained are coincident with the ones obtained by GIXD on pure water subphase and both scans are similar (Figure 7). These peaks show that the measured diffraction at water surface comes from 3D crystals or from multilayer formed at the air/pure water interface upon compression, as showed by the Q_z - Q_{xy} map of the diffraction data.

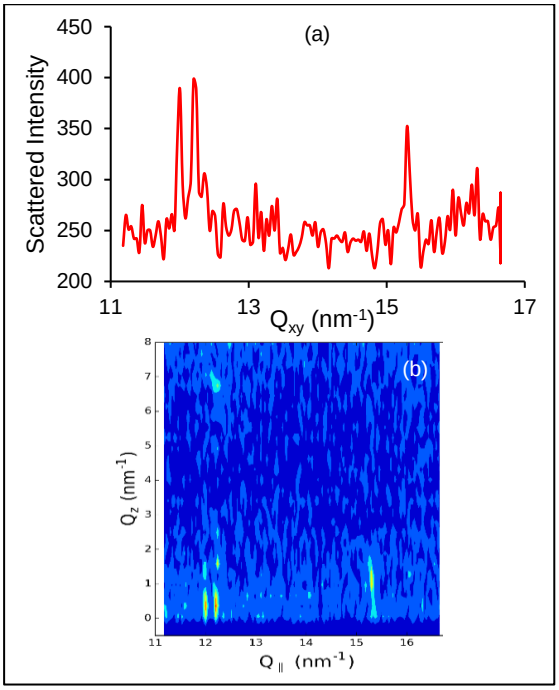

Figure 6 – GIXD spectrum: (a) Scattered Intensity vs Q_{xy}: (b) Qz vs $Q_{||}$. Note that $Q_{||}$=Q_{xy}.

After, it was performed GIXD on SW. It was performed several experiments (8 to 21) at different volumes, compression rates and relaxation times. The intervals of the scans were similar to the intervals chosen on the experiments on PW: the 9th and 11th were taken between Q_{xy}=9.0nm^{-1} – 17 nm^{-1}; the 13th in the interval of Q_{xy}=5.5nm^{-1} – 8.0nm^{-1}; the 15th, 17th and 19th between 7.0nm^{-1} and 8.6nm^{-1}; and the other ones (8th, 10th, 12th, 14th, 16th, 18th, 20th and 21st) from Q_{xy}=13.0 nm^{-1} to 18.0nm^{-1}.

As stated above on Chapter II.1 Langmuir Isotherms, the addition of NaCl to the pure water stabilizes the monolayer and consequently it was expected to find more peaks than the ones found on pure water subphase, which happens: the double number of the peaks found on the previous experiment (8) were found in this experiment (16). It was found 3 peaks between 7.40 nm^{-1} and 8.00 nm^{-1} at salt water subphase, comparing to pure water subphase, where only one peak was found on this interval; on salt water subphase, no peaks were found below 13.02 nm^{-1} and four peaks were found above 15.30 nm^{-1} (on pure water, four peaks were found below 13.0 nm^{-1} and no peaks were found above 15.30 nm^{-1}); the other nine peaks were found between 13.20 nm^{-1} and 15.30 nm^{-1}, comparing to two found on pure water. Four of these were only found on 3rd expansion: Q_{xy}=14.10 nm^{-1}, Q_{xy}=14.80 nm^{-1}, Q_{xy}=14.90 nm^{-1} and Q_{xy}=16.50 nm^{-1}. All the peaks on this subphase were found above the ESP value obtained for this subphase (23.3 mN m^{-1}).

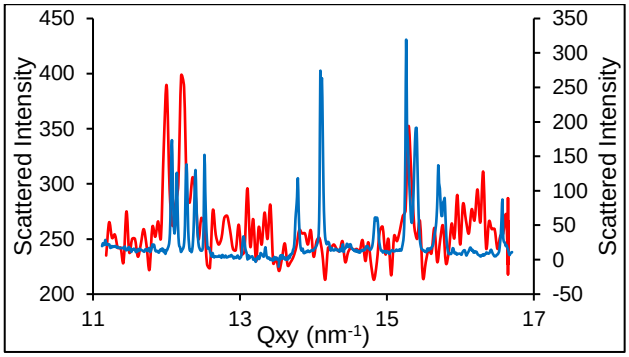

Figure 7 – Comparison of Bulk Powder diffraction (blue line; secondary axis) and Water Surface GIXD (Red line; principal axis).

2. Total Reflection X-ray fluorescence (TRXF)

TRXF was used to analyse the chemical composition of the interface of the monolayer of [C_{18}mim][NTf_2] since this technique is chemically sensitive. The measurement consists in recording a fluorescence spectrum, i.e. the number of photons for each energy in the x-ray range coming from the illuminated interface. The fluorescence spectrum can give a lot of information which can characterize the excitation source (position of elastic and inelastic scattering lines) and the samples. All the chemical elements present in the sample influence and contribute to the resulting spectrum.

In the present work, it was analyzed the sulfur content, since it is present in [NTf_2]$^-$, during a three-day experiment by its fluorescence energy emission (characteristic emitted energy of sulfur: 2.3 keV). This

is possible because the peak intensity depends on the amount of the atom present on the analyzed volume. [18] [19] The sulfur fluorescence intensity was normalized with elastic fluorescence intensity, the number of photons used for excitation. Besides being emitted, the incident x-ray light can be scattered on electrons. The most two significant types of scattering are elastic (Rayleigh) and inelastic (Compton) scattering. Light scattered by Elastic scattering has the same wavelength as the incident x-ray; whereas inelastic scattering has an increased wavelength (decrease of the energy). [18] [19] Both elastic and inelastic peaks depend on the incident x-ray. The Compton peaks appear at slightly lower energy than the Rayleigh peak on the fluorescence spectrum, so they are fitted at the left side of the curve; whereas the elastic is fitted at the incident energy (Figure 8). All the fluorescence emission lines derived from TRXF scan were fitted with Gaussian line shapes.

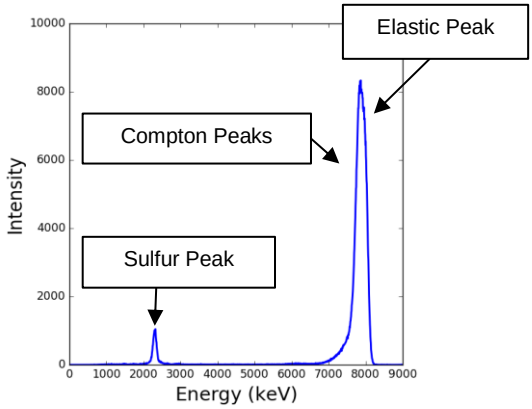

Figure 8 – Sulfur, Compton and Elastic Peak. Incident energy : 8keV.

As said before, the TRXF experiment lasted two days, in which: on the first day, it was performed a first compression and decompression; and on the second day, a recompression followed by a decompression. This experiment aimed to follow the evolution of the sulfur content during each compression (Figure 9).

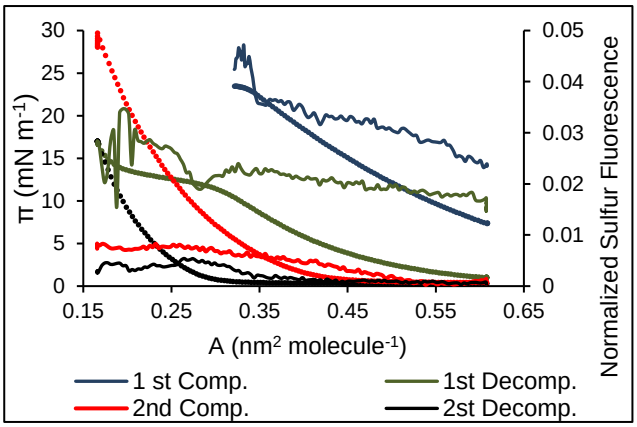

Figure 9 – Normalized Sulfur Fluorescence (plain curve) along compression and correspondent surface pressure (dotted curve).

From the results, it is observed that during the first compression, the sulfur fluorescence level is gradually rising due to increase in surface density, until the plateau is reached. At this moment, the surface pressure does not evolve, but there is a step increase of the sulfur fluorescence intensity. This happens due to crystal formation on the interface. This is in agreement with the appearance of crystalline-like structures on BAM images and peaks in GIXD. It is possible to say that crystal formation on the surface happens at this point.

At the beginning of decompression, it is first observed some perturbation on sulfur fluorescence. Then, at the end of the plateau, a big decrease of the fluorescence, followed by a small increase and gradual decrease until end of expansion. The big decrease of the fluorescence happens at the end of the plateau, that occurs at a surface pressure similar to the ESP value, meaning that at this point the crystalline-like structures disappear. The gradual decrease of sulfur fluorescence happens with the decrease of the crystals on the surface.

After one day, the monolayer was recompressed and decompressed. In this compression/ decompression cycle, it is observed a small increase of sulfur fluorescence, smaller than the compression/ decompression performed in the first day (fluorescence maximum difference in the compressions: 0.035; fluorescence maximum difference in the decompressions: 0.025).

Therefore, the sulfur fluorescence level decreases with the compressions and decompressions. This means that the quantity of anions at the surface are decreasing, so they are disappearing from the surface. This could happen due to dissolution of the anion in water, however the existence of an equilibrium isotherm contradicts its complete dissolution. However, (π-A) measurement and TRXF are not sensitive to the same element. The (π-A) isotherms are manly determined by the long chain cations; whereas, TRXF measures only the presence of $[NTf_2]^-$ at the interface. Thus, it can be concluded that long chain cations remain at the interface and the anions dissolves in the subphase

III. Conclusion and future remarks

Results from Langmuir Isotherms, on both subphases, PW and SW, showed clearly that $[C_{18}mim][NTf_2]$ is more stable comparing to others from its family, $[C_nmim][NTf_2]$ (n=12, 14 and 16), and to $[C_{18}mim][Cl]$ and $[C_{18}mim][PF_6]$. It was also proved that the addition of salt stabilizes the monolayer.

From the first compression/ decompression behaviour, it can be concluded that first compression induces reversible formation of crystals above the ESP: (π-A) isotherms show a gradual increase in surface pressure up to 0.27 $nm^2 molecule^{-1}$, where a plateau region appears (0.27-0.17 nm^2 $molecule^{-1}$), a highly compressible region, probably due the appearance of crystals at the surface; by the appearance of bright spots and a thicker film, BAM results suggest the existence of a monolayer in coexistence with multi-layered structures ; on GIXD experiments it is obtained peaks above the ESP value

and with the help of powder diffraction it can be concluded the diffraction comes from 3D crystals/ multilayer formed at the A/PW interface; on TRXF results, the step increase of sulfur fluorescence intensity, when the plateau is reached is also in agreement with the appearance of crystalline-like structures.

In the long term behaviour, an evolution of the layer is observed: the (π-A) isotherms shift to higher molecular areas and higher surface pressures, which suggests an evolution in the layer leading to a loss in area, attributed to a loss of molecules by dissolution on the subphase at the first sight. Although an equilibrium isotherm exists meaning that the dissolution is not complete; BAM results show a disappearance of the domains when the film is further compressed; the TRXF results of [C_{18}mim][NTf_2] suggest that the anions are disappearing from the interface by dissolution in water; this evolution can be due to a conformational change of the IL on water where anions are disappearing, leaving at the interface only long chain cation.

In future work, it would be interesting to perform BAM experiments on the same conditions used in the present work in order to obtain better images and to complement the present results. It would be also interesting to analyse [C_{18}mim][NTf_2] when further compressed by experiments such as Langmuir isotherms, BAM and X-ray experiments. This study could help to understand what happens to the monolayer. Besides the analysis of further compression, the study of the molecule for different relaxation times would be also interesting. It also would be interesting to study the behaviour at the interface of ILs with longer chains ([C_{20}mim]$^+$, [C_{22}mim]$^+$,…), for which dissolution is highly unlikely.

References

[1] R. Hayes, G. G. Warr, and R. Atkin, “Structure and Nanostructure in Ionic Liquids,” *Chem. Rev.*, vol. 115, no. 13, pp. 6357–6426, Jul. 2015.

[2] P. Wasserscheid and T. Welton, Eds., *Ionic Liquids in Synthesis*. Weinheim, FRG, 2002.

[3] Aldrich, “ChemFiles: Enabling Technologies,” vol. 5, no. 6, 2005.

[4] A. P. Tavares, O. Rodriguez, and E. A. Macedo, “New Generations of Ionic Liquids Applied to Enzymatic Biocatalysis,” in *Ionic Liquids - New Aspects for the Future*, InTech, 2013, pp. 539–556.

[5] L. Tamam, B. M. Ocko, H. Reichert, and M. Deutsch, “Checkerboard Self-Patterning of an Ionic Liquid Film on Mercury,” *Phys. Rev. Lett.*, vol. 106, no. 19, p. 197801, May 2011.

[6] H. Wu, M. Chen, Y. Fan, F. Elsebaei, and Y. Zhu, “Determination of rutin and quercetin in Chinese herbal medicine by ionic liquid-based pressurized liquid extraction–liquid chromatography–chemiluminescence detection,” *Talanta*, vol. 88, pp. 222–229, 2012.

[7] N. V. Plechkova *et al.*, “Applications of ionic liquids in the chemical industry,” *Chem. Soc. Rev.*, vol. 37, no. 1, pp. 123–150, 2008.

[8] T. Welton, “Room-Temperature Ionic Liquids. Solvents for Synthesis and Catalysis,” *Chem. Rev.*, vol. 99, no. 8, pp. 2071–2084, 1999.

[9] T. Kuboki, T. Okuyama, T. Ohsaki, and N. Takami, “Lithium-air batteries using hydrophobic room temperature ionic liquid electrolyte,” *J. Power Sources*, vol. 146, no. 1–2, pp. 766–769, 2005.

[10] A. Lewandowski and A. Świderska-Mocek, “Ionic liquids as electrolytes for Li-ion batteries—An overview of electrochemical studies,” *J. Power Sources*, vol. 194, no. 2, pp. 601–609, 2009.

[11] R. D. Rogers and K. R. Seddon, “Ionic Liquids--Solvents of the Future?,” *Science (80-.).*, vol. 302, no. 5646, pp. 792–793, 2003.

[12] L. Zhao, Y.-S. Hu, H. Li, Z. Wang, and L. Chen, “Porous Li4Ti5O12 Coated with N-Doped Carbon from Ionic Liquids for Li-Ion Batteries,” *Adv. Mater.*, vol. 23, no. 11, pp. 1385–1388, Mar. 2011.

[13] X. Bai, X. Li, and L. Zheng, “Chiral Ionic Liquid Monolayer-Stabilized Gold Nanoparticles: Synthesis, Self-Assembly, and Application to SERS,” *Langmuir*, vol. 26, no. 14, pp. 12209–12214, Jul. 2010.

[14] H. Jia *et al.*, “One-step synthesis and assembly of gold nanochains using the Langmuir monolayer of long-chain ionic liquids and their applications to SERS,” *CrystEngComm*, vol. 14, no. 8, pp. 2920–2925, 2012.

[15] I. Mukherjee, S. Mukherjee, B. Naskar, S. Ghosh, and S. P. Moulik, “Amphiphilic behavior of two phosphonium based ionic liquids,” *J. Colloid Interface Sci.*, vol. 395, pp. 135–144, Apr. 2013.

[16] E. J. M. Filipe *et al.*, “Crystalline-like structures and multilayering in Langmuir films of ionic liquids at the air–water interface,” *Chem. Commun.*, vol. 52, no. 32, pp. 5585–5588, 2016.

[17] B. J. Park, J. P. Pantina, E. M. Furst, M. Oettel, S. R. And, and J. Vermant, “Direct Measurements of the Effects of Salt and Surfactant on Interaction Forces between Colloidal Particles at Water−Oil Interfaces,” *Langmuir*, vol. 24, no. 5, pp. 1686–1694, 2008.

[18] M. Haschke, “XRF-Basics,” in *Laboratory Micro-X-Ray Fluorescence Spectroscopy*, 2014, pp. 1–17.

[19] B. Beckhoff, habil. B. Kanngießer, N. Langhoff, R. Wedell, and H. Wolff, *Handbook of Practical X-Ray Fluorescence Analysis*. Berlin, Heidelberg: Springer Berlin Heidelberg, 2006.